*Global and Stochastic Analysis* **DOI: 10.64837/GSA.13.3.10**
*Vol. 13 No. 3 (2026)*

*Received: 05th May 2026* *Revised: 26th June 2026* *Accepted: 30th June 2026*

# COMPARATIVE ANALYSIS OF FRONT AND REAR STAGNATION POINT FLOW OF ENGINE OIL

R. D. JAGADEESHA, M. KIRANKUMAR, M. J. SRIDEVI*, S. KEMPARAJU*, H. C. SHASHIKUMAR, K. C. JAGADEESHA, VIKAS K., AND REKHA J.

Abstract. The present investigation examines the stagnation point flow of a Casson hybrid nanofluid over a permeable, stretchable surface, accounting for heat sink/source and thermal radiation effects. The flow model incorporates unsteady flow, permeable walls, and Casson fluid rheology, and the hybrid nanofluid is prepared by mixing $Al_2O_3$ and Cu nanoparticles in engine oil. A set of nonlinear ordinary differential equations is solved using the Runge-Kutta-Felhberg method. Particular emphasis is placed on the flow behavior in the front and rear stagnation point regions. The results show that, for the front stagnation point flow, the velocity profile increases with higher values of the Casson parameter, whereas, for the rear stagnation point flow, the reverse-flow structure becomes more prominent as the Casson parameter increases. Furthermore, thermal radiation and heat generation significantly increase the temperature distribution and thickness of the thermal boundary layer. The comparative analysis shows that the thermal boundary layer is thicker in the rear stagnation point region than in the front stagnation point region. The outcomes provide valuable data on momentum and heat transfer mechanisms of hybrid nanofluids and can be used for thermal energy systems, polymer extrusion processes, coating technology, lubrication devices, and advanced cooling applications.

## 1. Nomenclature

| Symbol | Description | Symbol | Description |
|---|---|---|---|
| $k$ | Thermal conductivity | $s^*$ | Suction/blowing parameter |
| $U_e$ | Outer potential flow | $\mu$ | Dynamic viscosity |
| $\eta$ | Similarity variable | $Q_0$ | Strength of heat source/sink |
| $\theta(\eta)$ | Temperature profile | $Q^*$ | Heat source/sink parameter |
| Pr | Prandtl number | $(u, v)$ | Velocity components |
| $\nu$ | Kinematic viscosity | $v_w(t)$ | Wall permeability |
| $\rho$ | Density | $\dot{a}(t)$ | Stretching speed |
| $S$ | Unsteadiness parameter | $T$ | Temperature |
| $k^*$ | Mean absorption coefficient | $Rd$ | Radiation parameter |
| $d$ | Constant | $C_p$ | Specific heat |
| $f'(\eta)$ | Velocity profile | $p$ | Pressure |
| $(x, y)$ | Directions | $t$ | Time |
| $\sigma^*$ | Stephen-Boltzmann constant | $T_w$ | Temperature of the wall |
| $T_\infty$ | Ambient temperature | | |

2000 *Mathematics Subject Classification.* Primary: 76A05, 76Mxx; Secondary: 34B15, 76R05.

*Key words and phrases.* Hybrid nanofluid; Front-rear stagnation point flow; Stretching surface; Thermal radiation; Heat source/sink.

*Corresponding authors.

## 2. Introduction

Advanced heat transfer (HT) fluids, known as hybrid nanofluids (H-NFs), consist of two different types of nanoparticles dispersed in a conventional base fluid. Different nanoparticle types can give the fluid synergistic thermal properties that are not achievable with individual particles of those types. H-NFs are a recent area of study in thermal sciences due to their exceptional thermal conductivity, high heat capacity, and improved transport properties. The interaction among different nanoparticles and the carrier fluid creates complex HT phenomena, which can improve thermal efficiency in various engineering and energy applications. Kumar and Sharma [19] analysed the H-NF flow and HT over a permeable slider with a heat sink/source (H-SS). The chemically reactive and radiative H-NF flow due to moving flat plates was studied by Tejaswini et al. [23]. Sharma et al. [12] probed the HT and H-NF flow between two spinning disks. Waqas et al. [25] scrutinized the H-NF flow over a spinning disk with magnetohydrodynamic (MHD) effect. Waqas et al. [26] illustrated the H-NF flow and HT over a stretching surface (SS).

Stagnation point flow (SPF) is a fundamental boundary-layer flow in which the fluid velocity gradually decreases to zero at a point called the stagnation point. Strong momentum gradients form in this region, leading to pronounced variations in flow structure and transport properties. Studying SPF is significant because it provides a simplified model for the behavior of a fluid near impinging surfaces. Furthermore, external flow and boundary-layer development in the immediate vicinity of the stagnation region provide important insight into the momentum and HT processes in complex fluid systems. Turkyilmazoglu and Alotaibi [24] scrutinized the MHD SPF over a permeable surface in front and rear stagnation regions. Kattimani et al. [10] examined SPF of radiative Casson fluid across a spinning disk. Banakar et al. [5] discussed radiative effects on SPF of Casson micropolar fluid over a revolving disk. Naik et al. [15] investigated SPF of a Boger fluid due to a spinning disk. Rahman et al. [19] deliberated SPF of nanofluids over a stretching sheet.

A surface-stretching flow has attracted considerable interest in boundary-layer theory because of the distinctive fluid dynamics it exhibits. If the surface is continually extended in its own plane, the neighboring fluid is drawn along, and a boundary layer develops and evolves. The stretching motion alters the fluid's momentum distribution and strongly influences heat-transfer behavior near the surface. These flow patterns lend themselves to a clear mathematical description of transport phenomena in moving-boundary systems. Therefore, surface flows are often utilized to study how different physical parameters affect the temperature and velocity distributions in non-Newtonian and Newtonian fluids. Sharma et al. [20] analysed the mass and HT on MHD flow of micropolar fluid over a SS. Kumar [13] examined the H-NF over a SS with radiative effect. Kumar et al. [4] probed the flow of Casson fluid over a SS with thermal radiation (TR) and MHD impact. Sureshkumar et al. [22] discussed the Boger fluid flow over a curved SS. Goud et al. [18] scrutinized the micropolar fluid flow over a SS.

Thermal radiation is a form of HT due to the emission and absorption of electromagnetic energy by matter at a finite temperature. Conduction and convection require a material medium, but radiative HT does not. Radiative HT is also more significant at high temperatures. In boundary-layer flows, TR alters the energy transport process, adding an extra heat flux to the fluid system. This can thus notably influence temperature distributions and the formation of thermal boundary layers. The inclusion of radiative effects is indispensable for obtaining realistic predictions of the HT behavior of high-temperature fluid flow problems. Kumar et al. [7] studied the reactive fluid flow subjected to two parallel disks with TR effect. Kumar et al. [11] scrutinized the HT and nanofluid flow over a vertical plate under TR effect. Megahed et al. [14] analysed the effects of TR on the MHD fluid flow over a SS. Kumar et al. [3] investigated the Casson fluid flow across an exponentially SS with TR effect. Pai et al. [17] discussed the effect of TR on the flow of Casson fluid between parallel plates

Heat absorption from the fluid is called a heat sink, and internal heat generation within the fluid is called a heat source. The thermal boundary layer properties and temperature distribution are changed by the addition of an H-SS effect, which affects the HT performance of the system. It is widely used in nuclear reactors, chemical processing, energy storage and thermal management technology. Srilatha et al. [21] studied the nanofluid flow past a rough revolving disk with an H-SS effect. Othman et al. [16] investigated the H-SS effect on H-NF over a shrinking surface. Banakar et al. [6] examined the H-SS effect on the tetra HNF between two active parallel plates. Agrawal et al. [2] analysed the effect of H-SS on the flow of H-NF over a permeable SS. Farooq et al. [8] discussed the impact of H-SS on HT and H-NF flow over a rotating disk.

While many of the earlier studies have examined stagnation-point flow, SSs, Casson fluids, TR, and H-NFs separately, the synergistic effects of these fluid phenomena on front and rear SPF remain largely unexplored. The novelty of the present work is that it investigates the comparative behavior of front and rear SPF of a Casson H-NF ($Cu - Al_2O_3$) past a permeable SS. In addition, the simultaneous consideration of TR and internal H-SS effects provides a more realistic model of high-temperature industrial processes. The present investigation highlights the unique momentum and heat transfer features of the forward and rear stagnation regions and differs from traditional stagnation-point studies of a single flow configuration. The outcomes may provide deeper insight into the dynamics of non-Newtonian H-NFs and help design better cooling systems, coating processes, polymer processing, and thermal energy conversion devices.

## 3. Mathematical analysis

In the present model, the $u$ and $v$ are the velocity components along the direction $x$ and $y$ respectively. $U_e$ is the velocity at the stagnation point on the outside and $T$ and $T_w$ are the fluid and wall temperatures. The Casson H-NF consists of a mixture of Cu and $Al_2O_3$ nanoparticles in engine oil. The TR effect is represented by the radiation parameter, $Rd$, and the H-SS parameter is represented by $Q^*$. In addition, the symbols $\beta$, $S$, and $s^*$ denote the Casson parameter, unsteadiness parameter and suction/blowing parameter, respectively. Figure 1 illustrates the flow representation. The governing equations are given by (See [24]),

(1)
$$\frac{\partial v}{\partial y} + \frac{\partial u}{\partial x} = 0,$$

(2)
$$v\frac{\partial u}{\partial y} - U_e\frac{\partial U_e}{\partial x} + u\frac{\partial u}{\partial x} + \frac{\partial u}{\partial t} = \frac{\partial U_e}{\partial t} + \nu_{hnf}\left(\frac{\partial^2 u}{\partial x^2} + \frac{\partial^2 u}{\partial y^2}\right)\left(\frac{1}{\beta} + 1\right),$$

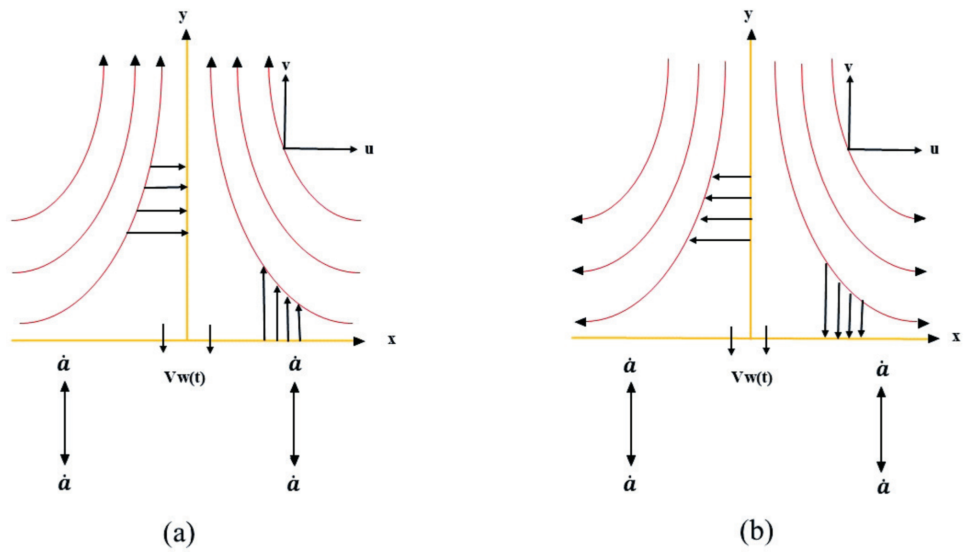


FIGURE 1. **(a)** Rear stagnation point flow **(b)** Front stagnation point flow.

(3)
$$v\frac{\partial v}{\partial y}+\frac{1}{\rho_{hnf}}\frac{\partial p}{\partial y}+u\frac{\partial v}{\partial x}+\frac{\partial v}{\partial t}=\nu_{hnf}\left(\frac{\partial^2 v}{\partial x^2}+\frac{\partial^2 v}{\partial y^2}\right)\left(\frac{1}{\beta}+1\right),$$

(4)
$$v\frac{\partial T}{\partial y}+\frac{\partial T}{\partial t}+u\frac{\partial T}{\partial x}=\frac{k_{hnf}}{(\rho C_p)_{hnf}}\frac{\partial^2 T}{\partial y^2}+\frac{1}{(\rho C_p)_{hnf}}Q_0(T-T_\infty)+\frac{1}{(\rho C_p)_{hnf}}\frac{16\sigma^* T_\infty^3}{3k^*}\frac{\partial^2 T}{\partial y^2}.$$

The corresponding boundary conditions are given by,

$$\left.\begin{aligned}&u=0, T=T_w,\ v=-v_w(t),\quad at\quad y=a\,(t)\,,\\&T=T_\infty, u=U_e(t),\quad as\quad y\to\infty.\end{aligned}\right\}\tag{5}$$

The following are the suitable similarity transformations,

$$\left.\begin{aligned}&\eta_t=-\frac{\dot{a}(t)}{a(t)}(\eta+1),\ u=\frac{\nu_f x}{a^2(t)}f'(\eta),\ \frac{1}{a(t)}=\eta_y,\\&v=-\nu_f\frac{1}{a(t)}f(\eta), \eta=-\left(1-\frac{y}{a(t)}\right),\ p=\frac{\rho_f\nu^2}{a^2(t)}P(\eta),\\&U_e(x,t)=\nu_f\frac{x}{a^2(t)}d, \theta(\eta)=\frac{T-T_\infty}{T_w-T_\infty}.\end{aligned}\right\}\tag{6}$$

The solved governing equations are given by,

$$\frac{\nu_{hnf}}{\nu_f}\left(1+\frac{1}{\beta}\right)f'''+ff''-f'^2+S\left(f'+\left(\frac{\eta+1}{2}\right)f''-d\right)+1=0,\tag{7}$$

$$\frac{(\rho C_p)_f}{(\rho C_p)_{hnf}}\left(\frac{k_{hnf}}{k_f}+4Rd\right)\theta''+\Pr S\left(\frac{\eta+1}{2}\right)\theta'+\Pr f\theta'+\Pr\frac{(\rho C_p)_f}{(\rho C_p)_{hnf}}Q^*\theta=0.\tag{8}$$

The reduced boundary conditions are given by,

$$
\left.\begin{aligned}
&f(0) = -s^*\frac{S}{2},\ f'(0) = 0, \theta(0) = 1, \quad \text{at} \quad a(t) = 0,\\
&f'(\infty) = d, \theta(\infty) = 0, \quad \text{at} \quad y \to \infty.
\end{aligned}\right\} \tag{9}
$$

The dimensionless parameters are given by,

$$
\left.\begin{aligned}
&Rd = \frac{4\sigma^* T_\infty^3}{3k^* k_f},\ \Pr = \frac{\nu_f (\rho C_p)_f}{k_f},\ Q^* = \frac{a^2(t) Q_0}{(\rho C_p)_f \nu_f},\\
&S = 2\frac{\dot{a}(t) a(t)}{\nu_f},\ s^* = \frac{v_w(t)}{\dot{a}(t)},
\end{aligned}\right\} \tag{10}
$$

where $S$ denotes either a ($S < 0$) backward-moving surface or a ($S > 0$) forward-moving surface. The wall can move, but is impermeable in the particular situation of $s^* = 1$, i.e., $\nu_w(t) = -\dot{a}(t)$. Therefore, blowing is represented by $s^* > 1$, whereas suction is denoted by $s^* < 1$. The thermophysical properties are given by,

$$
\left.\begin{aligned}
&\rho_{hnf} = ((1-\phi_1)\rho_f + \phi_1 \rho_{p1})(1-\phi_2) + \phi_2 \rho_{p2},\\
&\mu_{hnf} = \frac{\mu_f}{(1-\phi_2)^{2.5}(1-\phi_1)^{2.5}},\\
&(\rho C_p)_{hnf} = ((\rho C_p)_f (1-\phi_1) + \phi_1 (\rho C_p)_{p1})(1-\phi_2) + (\rho C_p)_{p2}\phi_2,\\
&k_{hnf} = k_{nf}\left(\frac{k_{p2} - 2\phi_2(k_{nf} - k_{p2}) + 2k_{nf}}{k_{p2} + \phi_2(k_{nf} - k_{p2}) + 2k_{nf}}\right),\\
&k_{nf} = k_f\left(\frac{k_{p1} - 2\phi_1(k_f - k_{p1}) + 2k_f}{k_{p1} + \phi_1(k_f - k_{p1}) + 2k_f}\right).
\end{aligned}\right\} \tag{11}
$$

## 4. Methodology

The Runge–Kutta–Fehlberg $4^{\text{th}}$–$5^{\text{th}}$ (RKF-45) method is a widely used numerical approach for solving a set of coupled nonlinear ordinary differential equations (ODEs). It combines Runge-Kutta 4th- and 5th-order schemes to estimate the local truncation error and automatically adjust the step size during computation. This adaptive step-size control improves both accuracy and efficiency in the solution, especially for boundary-layer flow problems with strong nonlinearity. The transformed ODEs were solved numerically using the RKF-45 technique with the prescribed boundary conditions, which ensured the accuracy, stability, and convergence of the numerical solutions in the computational domain. The following assumptions are considered:

$$
\lambda_1 = f(\eta), \lambda_2 = f'(\eta), \lambda_3 = f''(\eta), \lambda_4 = \theta(\eta), \lambda_5 = \theta'(\eta).\} \tag{12}
$$

Substituting the considered values in Eqs. (7) and (8) and the solved boundary condition Eq. (9),

(13)

$$
\lambda_3' = -\frac{1}{\frac{\nu_{hnf}}{\nu_f}\left(1+\frac{1}{\beta}\right)}\left(\lambda_1\lambda_3 - \lambda_2^2 + S\left(\lambda_2 + \left(\frac{\eta+1}{2}\right)\lambda_3 - d\right) + 1\right),
$$

(14)

$$\lambda_5' = -\frac{1}{\frac{(\rho C_p)_f}{(\rho C_p)_{hnf}}\left(\frac{k_{hnf}}{k_f} + 4Rd\right)}\left(\Pr S\left(\frac{\eta+1}{2}\right)\lambda_5 + \Pr\lambda_1\lambda_5 + \Pr\frac{(\rho C_p)_f}{(\rho C_p)_{hnf}}Q^*\lambda_4\right).$$

The corresponding boundary conditions are,

$$\left.\begin{aligned} &\lambda_2(0) = 0, \lambda_1(0) + s^*\frac{S}{2} = 0, \lambda_4(0) - 1 = 0,\\ &\lambda_2(\infty) - d = 0, \lambda_4(\infty) = 0. \end{aligned}\right\} \quad (15)$$

## 5. Result and discussion

The transformed ODEs were solved employing RKF-45 to examine the impact of the controlling parameters on the momentum and HT characteristics of the Casson H-NF. Particular attention was devoted to comparing the behaviour of front SPF ($d = 1$) and rear SPF ($d = -1$) over the permeable SS. The influences of the Casson parameter $\beta$, unsteadiness parameter $S$, suction/blowing parameter $s^*$, H-SS parameter $Q^*$, and radiation parameter $Rd$ on the momentum and thermal distributions were analysed systematically. The graphical results presented in Figures 2–7 provide a comprehensive description of the flow and thermal boundary-layer development and reveal the distinct transport mechanisms associated with the front and rear stagnation point regions. Table 1 illustrates the nanoparticles and base fluid's thermophysical values.

Figure 2 shows that the velocity profile $f'(\eta)$ for front and rear stagnation-point flows ($d = 1$ and $d = -1$) is influenced by the $\beta$. It is noted that the velocity distribution in

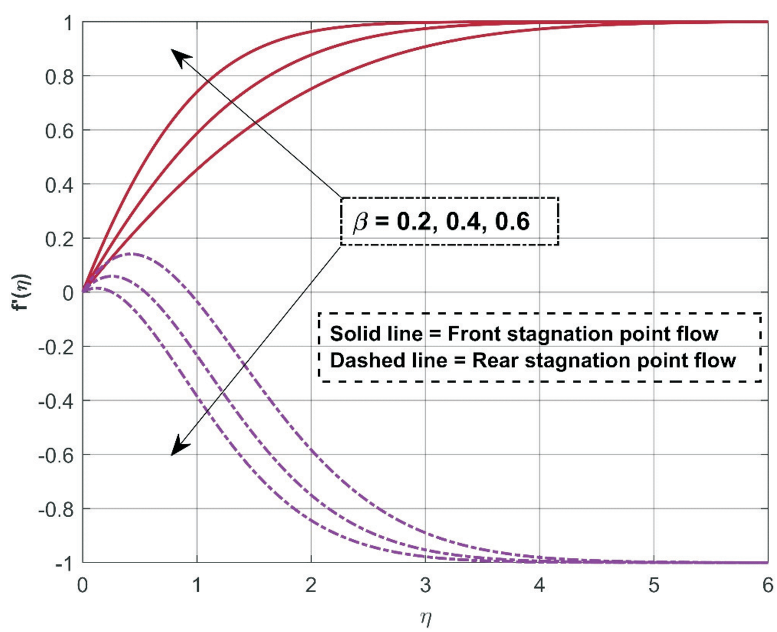


Figure 2. Consequence of $\beta$ on $f'(\eta)$.

the front stagnation-point region improves with increasing $\beta$, from 0.2 to 0.6, meaning that the fluid reaches the free-stream condition faster. This is because larger $\beta$ values reduce the yield-stress properties of the Casson fluid, resulting in less resistance to flow and greater momentum transfer. By contrast, in the stagnation-point region at the back of the profile, as $\beta$ increases, the reverse-flow features become more pronounced, and the velocity profiles tend to converge toward the asymptotic solution $f'(\eta) = -1$ more rapidly. This causes the momentum boundary-layer thickness to decrease and enhances momentum diffusion in both stagnation regions, thus higher $\beta$ values.

The effect of the unsteadiness parameter $S$ on the $f'(\eta)$ for the front ($d = 1$) and rear ($d = -1$) stagnation-point flows is shown in Figure 3. All cases correspond to $S > 0$ (forward-moving surface). It is clear that $S = 5$ yields a better velocity distribution in the front stagnation-point region than $S = 1$, thereby bringing the fluid to the free-stream state more quickly. Physically, a higher forward surface motion imparts more momentum to the adjacent fluid layers and strengthens the boundary-layer flow. In the rear stagnation-point region, increasing $S$ intensifies the reverse-flow structure, and the velocity profiles approach the asymptotic value of $f'(\eta) = -1$ more rapidly. As a result, higher values of $S$ increase momentum transport and decrease the momentum boundary-layer thickness in both stagnation regions.

The effect of the $s^*$ on the $f'(\eta)$ of the front ($d = 1$) and rear ($d = -1$) stagnation-point flows is shown in Figure 4. Cases of $s^* = -1.5$ and $s^* = 0.1$ represent suction, and $s^* = 1.5$ represents blowing. The results show that the velocity distribution decreases throughout the boundary layer in both the upstream and downstream stagnation regions as $s^*$ increases. Physically, fluid injection through the porous surface adds fluid near the wall, thereby diminishing momentum transfer from the SS, which in turn slows the flow acceleration. A similar behavior is observed in the rear stagnation-point region: increasing $s^*$ leads to more pronounced negative flow and a thicker momentum boundary layer. Hence, higher values of $s^*$ reduce the velocity field and slow the approach to the free stream in front of and behind the stagnation-point flows.

The influence of the $S$ on the $\theta(\eta)$ is shown for both the front ($d = 1$) and rear ($d = -1$) stagnation-point flows in Figure 5. All cases are for a forward-moving surface ($S > 0$). From the above observation, it is found that a higher value of $S$ leads to a lower temperature distribution in the thermal boundary layer in both stagnation regions. From a physical point of view, greater forward surface motion increases convective transport and thus the removal of thermal energy from the vicinity of the wall. As a result, the fluid temperature drops and the thermal boundary layer gets thinner. The same trend applies to both flows, but the rear stagnation-point flow has a relatively thick thermal boundary layer compared to the front SPF, owing to the presence of reverse-flow characteristics and lower thermal transport.

The effect of the $Q^*$ on the $\theta(\eta)$ is shown in Figure 6 for the SPF on the front ($d = 1$) and the rear ($d = -1$). The temperature distribution is higher for larger $Q^*$ in both flow regions, as seen when moving from $Q^* = -1$ to $Q^* = 0.8$. Physically, negative $Q^*$ indicates heat absorption, drawing heat from the fluid and decreasing the thermal boundary-layer thickness. Positive $Q^*$ indicates internal heat generation, which adds thermal energy to the system and raises the fluid temperature. Thus, the thicker the thermal boundary layer, the higher the $Q^*$. While both stagnation regions show similar characteristics, the rear stagnation-point flow has relatively higher temperatures, attributed to its thicker thermal boundary layer.

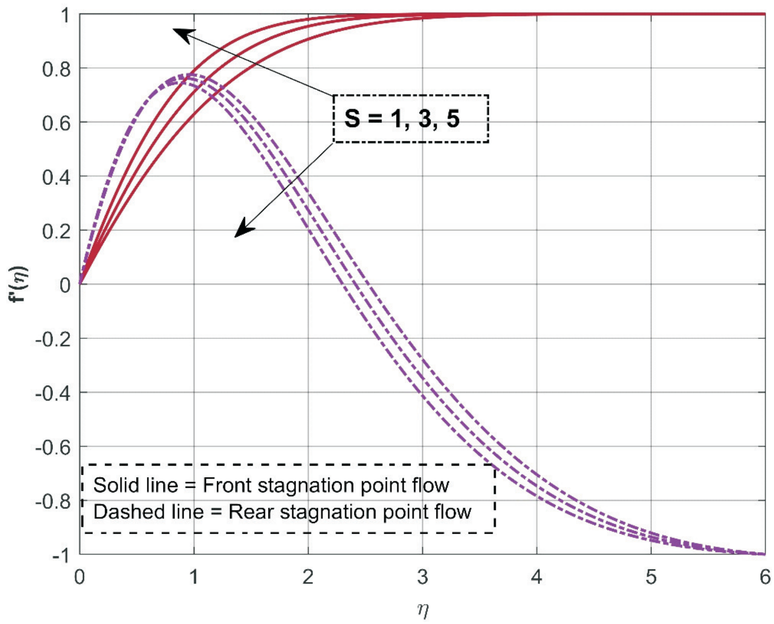


FIGURE 3. Consequence of $S$ on $f'(\eta)$.

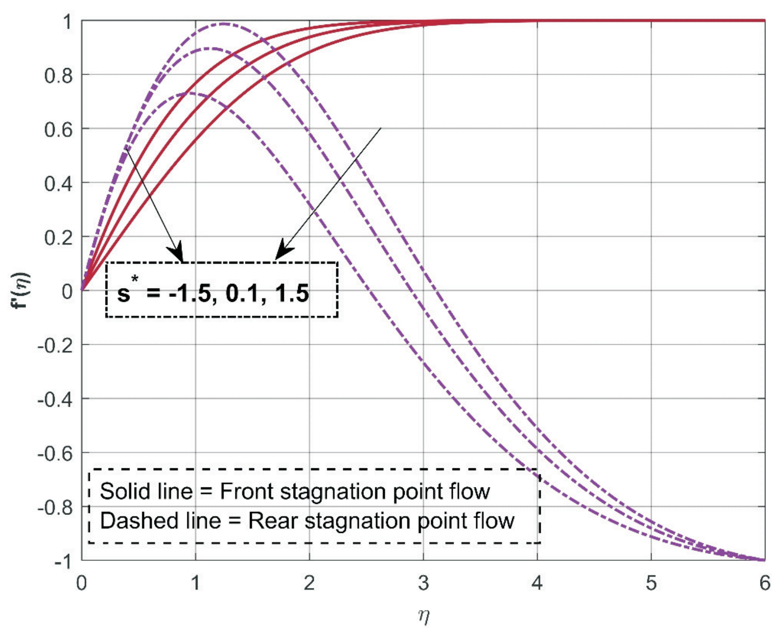


FIGURE 4. Consequence of $s^*$ on $f'(\eta)$.

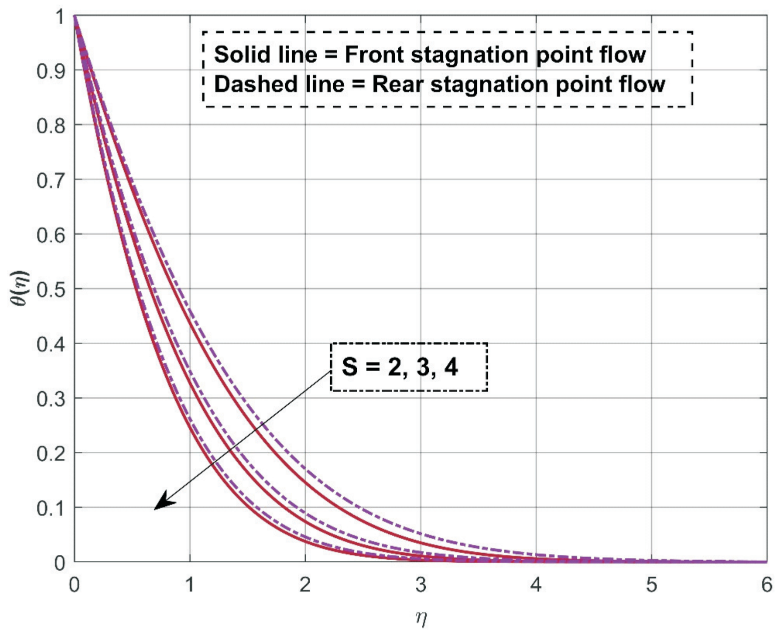


Figure 5. Consequence of $S$ on $\theta(\eta)$.

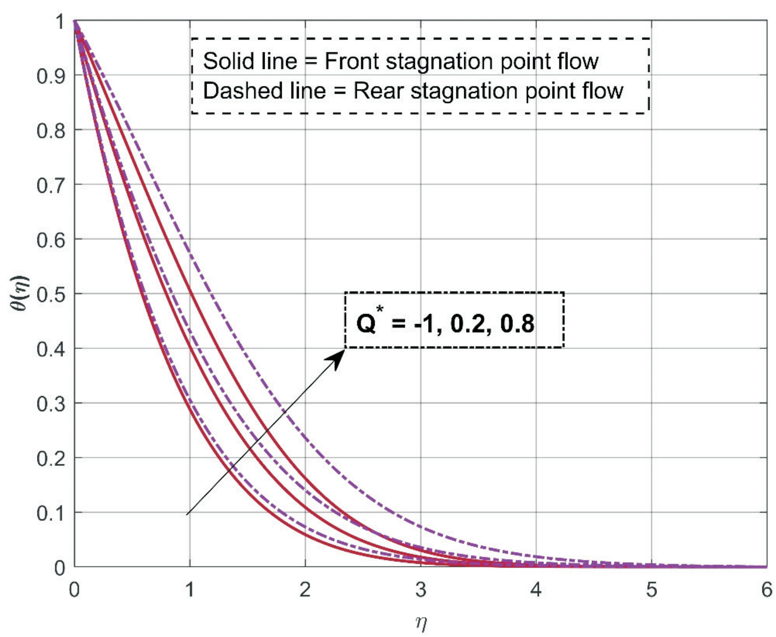


Figure 6. Consequence of $Q^*$ on $\theta(\eta)$.

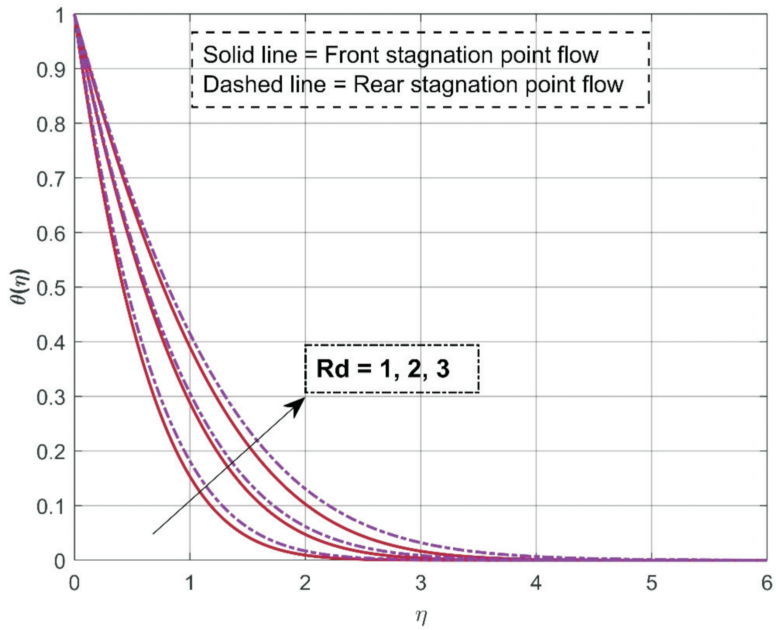


FIGURE 7. Consequence of $Rd$ on $\theta(\eta)$.

Figure 7 shows the consequence of the radiation parameter, $Rd$, on the $\theta(\eta)$ for the front ($d = 1$) and rear ($d = -1$) SPFs. It is observed that increasing $Rd$ from 1 to 3 improves the temperature distribution and increases the thickness of the thermal boundary layer in both flow regions. In an actual flow, larger values of $Rd$ enhance radiative HT in the fluid, which in turn increases the effective thermal diffusivity and slows heat loss from the boundary layer. As a result, the fluid stores more thermal energy, leading to higher temperatures throughout the domain. The same behavior is observed in both stagnation regions, but the temperature is higher in the rear SPF, suggesting that the thermal boundary layer is thicker and HT is less than in the front SPF.

TABLE 1. The thermophysical values of base fluid and nanoparticles (See [9]).

| **Properties** | **Density** | **Thermal conductivity** | **Specific heat** |
|---|---|---|---|
| Engine oil (Base fluid) | 884 | 0.144 | 1910 |
| Cu | 8963 | 400 | 385 |
| $Al_2O_3$ | 3970 | 40 | 765 |

## 6. Conclusion

The front and rear SPF of a Casson H-NF with the mixture of $Al_2O_3$ and Cu nanoparticles in the engine oil, with the consideration of the H-SS and TR effect over a permeable SS, was investigated. The system of nonlinear ODEs is solved by utilizing the RKF-45. A focus was given on the comparison of the momentum and HT features of the front and rear stagnation point regions. The consequence of the forward-moving surface, suction/blowing, H-SS, and radiation parameters on the temperature and velocity profiles was systematically investigated to gain a thorough understanding of the HT and flow behavior of the H-NF. The following are the main outcomes of the study.

The $\beta$ increases the $f'(\eta)$ in the front SPF region ($d = 1$), and improves the reverse-flow characteristics in the rear SPF region ($d = -1$), resulting in different velocity responses in the two flow configurations.

An increase in the $S \quad (S > 0)$ speeds up the fluid flow while decreasing the thickness of the thermal boundary layer, which means that the convective cooling capability improves.

The $f'(\eta)$ is suppressed in both front and rear SPFs for increasing values of the $s^*$, and the free-stream condition is not reached until a later time, leading to a thicker momentum boundary layer.

HT is strongly affected by the $Q^*$, the positive $Q^*$ values enhance the $\theta(\eta)$ and thermal boundary-layer thickness, while negative $Q^*$ values enhance cooling by removing heat from the fluid.

The $\theta(\eta)$ is significantly increased, and the thermal boundary layer is thickened, due to TR in both stagnation points, with the rear SPF having a comparatively thicker thermal boundary layer than the front SPF.

## Acknowledgments

We would like to express our gratitude to anonymous Reviewers for their valuable comments.

## References

1. N. H. Abd Rahman, N. Bachok and H. Rosali, *MHD Stagnation Point Flow over a Nonlinear Stretching/Shrinking Sheet in Nanofluids*, J. Adv. Res. Fluid Mech. Therm. Sci., 76 (2020), 139–152.
2. P. Agrawal, P. K. Dadheech, R. N. Jat, D. Baleanu and S. D. Purohit, *Radiative MHD hybrid-nanofluids flow over a permeable stretching surface with heat source/sink embedded in porous medium*, Int. J. Numer. Methods Heat Fluid Flow, **31** (2021), 2818–2840.
3. K. Anantha Kumar, V. Sugunamma and N. Sandeep, *Effect of thermal radiation on MHD Casson fluid flow over an exponentially stretching curved sheet*, *J. Therm. Anal. Calorim.*, **140** (2020), 2377–2385.
4. K. Anantha Kumar, A. C. Venkata Ramudu, V. Sugunamma and N. Sandeep, *Effect of non-linear thermal radiation on MHD Casson fluid flow past a stretching surface with chemical reaction*, Int. J. Ambient Energy, **43** (2022), 8400–8407.
5. V. R. Banakar, K. Karthik, S. P. Jena and R. S. V. Kumar, *Optimizing and understanding complex relationships between micro-inertia and spin gradient viscosity in off-centered stagnation point flow*, Dyn. Atmospheres Oceans, **114** (2026), Article Id: 101660.
6. V. R. Banakar, B. S. Sanju, E. H. Kumcu, I. E. Sarris, P. Kattimani and R. J. Punith Gowda, *Comparative analysis of thermal radiation models to assess heat transfer efficacy in active parallel plates using operational matrix of Legendre polynomials*, Mod. Phys. Lett. B, (2026), DOI: 10.1142/S0217984926501666.
7. M. Bharath Kumar, M. Vijaya Kumar, M. Nagapavani, M. Varuna and P. Siva Kota Reddy, *Artificial neural network and Sigmoid polynomial-based method for chemically reactive fluid flow mechanism between upper stationary and lower rotating disk*, International Journal of Thermofluids, 34 (2026), Article Id: 101646, 18 Pages.
8. U. Farooq, M. Imran, S. Noreen, N. Fatima and T. Muhammad, *Heat Transfer Performance of Hybrid Nanofluid Radiative Flow via a Rotating Disk With Heat Source–Sink Effects and Response Surface Methodology*, Math. Meth. Appl. Sci., (2025), DOI: 10.1002/mma.10821.

9. A. Hussain, M. Arshad, A. Hassan, A. Rehman, H. Ahmad, J. Baili and T. N. Gia, *Heat transport investigation of engine oil based rotating nanomaterial liquid flow in the existence of partial slip effect*, Case Stud. Therm. Eng., **28** (2021), Article Id: 101500.
10. P. Kattimani, K. Karthik, G. Singh, A. Kulshreshta, R. N. Kumar and R. J. Punith Gowda, *Artificial Neural Network Approach for Homogeneous-Heterogeneous Catalytic Reaction in Off-Centered Stagnation Flow*, *ZAMM Zeitschrift fur Angewandte Mathematik und Mechanik*, **106**(5) (2026), Article Id: e70453.
11. M. A. Kumar, Y. D. Reddy, V. S. Rao and B. S. Goud, *Thermal radiation impact on MHD heat transfer natural convective nano fluid flow over an impulsively started vertical plate*, *Case Stud. Therm. Eng.*, **24** (2021), Article Id: 100826.
12. V. V. Kumar and R. P. Sharma, *Taguchi design approach for thermal enhancement in time-varying fluid injection of MXene bi-hybrid nanofluid-lubricated porous slider*, Physics of Fluids, **37** (2025), Article Id: 093128.
13. T. S. Kumar, *Hybrid nanofluid slip flow and heat transfer over a stretching surface*, Partial Differ. Equ. Appl. Math., **4** (2021), Article Id: 100070.
14. A. M. Megahed, M. G. Reddy and W. Abbas, *Modeling of MHD fluid flow over an unsteady stretching sheet with thermal radiation, variable fluid properties and heat flux*, Math. Comput. Simul., **185** (2021), 583–593.
15. L. S. Naik, D. G. Prakasha, C. G. Jagannatha, K.C. Jagadeesha and S. K. Abhilasha, *Artificial neural network approach to analyse the effect of solvent fraction on off-centered stagnation flow towards a rotating disk*, Therm. Adv., **7** (2026), Article Id: 100144.
16. M. N. Othman, A. Jedi, N. A. A. Bakar, *MHD Flow and Heat Transfer of Hybrid Nanofluid over an Exponentially Shrinking Surface with Heat Source/Sink*, Appl. Sci., **11**(17) (2021), Article Id: 8199.
17. N. P. Pai, B. Devaki, Pareekshith, V. S. Sampath Kumar and K. R. vasanth, *Radiation effect on MHD Casson Fluid Flow between Parallel Plates of Different Permeability*, Global and Stochastic Analysis, **10**(2) (2023), 135–149.
18. B. Shankar Goud and M. M. Nandeppanavar, *Ohmic heating and chemical reaction effect on MHD flow of micropolar fluid past a stretching surface*, Partial Differ. Equ. Appl. Math., **4** (2021), Article Id: 100104.
19. R. P. Sharma, B. K. Barik, V. V. Kumar and A. Sharma, *Illustration of low oscillating magnetic field on sodium alginate-based hybrid nanofluid flow between two revolving disks: An artificial neural network-based study*, Eng. Appl. Artif. Intell., **155** (2025), Article Id: 111101.
20. S. Sharma, A. Dadheech, A. Parmar, J. Arora, Q. Al-Mdallal and S. Saranya, *MHD micro polar fluid flow over a stretching surface with melting and slip effect*, Scientific Reports, **13** (2023), Article number: 10715.
21. P. Srilatha, S. K. Abhilasha, D. G. Prakasha, M. Radhika, K. V. N. Shanmukha Sid and B. S. Sanju, *Numerical and empirical approach to study the influence of high-frequency oscillating magnetic field and nanoparticle aggregation on rough revolving disk in a porous medium*, International Journal of Thermofluids, **34** (2026), Article Id: 101631.
22. S. Sureshkumar, K. M. Devendraiah, S. Prasanna Rani, C. G. Jagannatha, L. Sing Naik and K. C. Jagadeesha, *Impact of Generation and Absorption of Heat on the Flow of Boger Fluid Past A Curved Stretching Sheet: A Non-Similarity Solution Approach*, Global and Stochastic Analysis, **13**(1) (2026), 49–68.
23. G. K. Tejaswini, K. Vinutha, J. K. Madhukesh, P. Siva Kota Reddy and Umair Khan, *RKF45 optimization for the boundary layer hybrid nanofluid flows of stationary and moving flat plates with chemical reactions*, Discover Applied Sciences, **8** (2026), Article Number: 334, 18 Pages.
24. M. Turkyilmazoglu and A. Alotaibi, *MHD Front and rear stagnation-point flow of a moving permeable flat surface*, Phys. Nonlinear Phenom., **487** (2026), Article Id: 135075.
25. H. Waqas, U. Farooq, R. Naseem, S. Hussain and M. Alghamdi, *Impact of MHD radiative flow of hybrid nanofluid over a rotating disk*, Case Stud. Therm. Eng., **26** (2021), Article Id: 101015.
26. H. Waqas, U. Farooq, D. Liu, M. Abid, M. Imran and T. Muhammad, *Heat transfer analysis of hybrid nanofluid flow with thermal radiation through a stretching sheet: A comparative study*, Int. Commun. Heat Mass Transf., **138** (2022), Article Id: 106303.

R. D. Jagadeesha, Department of Mathematics, Government First Grade College for Women, Holenarasipura-573 211, India.
*Email address*: jagdeesh25@gmail.com

M. Kirankumar, Department of Mathematics, Vidyavardhaka College of Engineering, Mysuru-570 006, India.
*Email address*: kiran.maths@vvce.ac.in

M. J. Sridevi, Department of Mathematics, Government First Grade College for Women, Hassan-573 201, India.
*Email address*: thanusri.j@gmail.com

S. Kemparaju, Department of Mathematics, Government First Grade College, Ramanagara-562 159, India.
*Email address*: skemparaju74@gmail.com

H. C. Shashikumar, Department of Mathematics, Government First Grade College, Tiptur-572 201, India.
*Email address*: shashikumarhc30@gmail.com

K. C. Jagadeesha, Department of Mathematics, Government First Grade College, Tumkur-572 102, India.
*Email address*: kcjagadish.09@gmail.com

Vikas K., Department of Mathematics, Bapuji Institute of Engineering and Technology, Davanagere-577 004, India.
*Email address*: vikasprt@gmail.com

Rekha J., Department of Mathematics, Cambridge Institute of Technology, Bengaluru-560 036, Karnataka, India.
*Email address*: rekha.maths@cambridge.edu.in